SCIENCE CHINA
Technological Sciences

•Article•

January 2023 Vol.66 No.1: 193–203
https://doi.org/10.1007/s11431-022-2209-9

A novel preheating method for the Li-ion battery using supercooled phase change materials

FANG XuanYi, NONG XinLu, LIAO ZhiRong* & XU Chao

Key Laboratory of Power Station Energy Transfer Conversion and System of Ministry of Education, School of Energy, Power and Mechanical Engineering, North China Electric Power University, Beijing 102206, China

Received May 25, 2022; accepted September 15, 2022; published online November 25, 2022

The Li-ion battery is widely used in power tools, energy storage systems, and electric vehicles. In reality, battery thermal management is essential to control the battery temperature within a specific temperature range. Although research has shown that preheating the battery at low temperatures on cold days can improve output performance significantly, few efforts have been made to study the preheating method in-depth. As a result, this research proposes two preheating designs for cylindrical batteries with supercooled phase change materials: Single- and dual-phase change material (PCM) designs. A mathematical model is developed to analyze the effect of the PCM layer's height, thickness, and mass on the preheating effect for seven candidate PCMs with high supercooling degrees. Furthermore, the economic efficiency of the single-PCM design with different PCMs is compared. In addition, the optimal ratio of the PCMs' height for the dual-PCM design is investigated. Eventually, the improvement of the battery's output performance is discussed. The results reveal that the proposed designs can effectively preheat the battery with a temperature rise higher than 10°C. The single-PCM design using $LiNO_3 \cdot 3H_2O$ shows the best preheating ability, while $CH_3COONa \cdot 3H_2O$ is the most economical. Although the dual-PCM design cannot outperform the single-PCM design, it can preheat the battery twice and show better flexibility. Compared with the battery without preheating, a 26650-format battery with the single-PCM design can prolong the operating time by 38.8 min and save the electric quantity by 2.1 A h; while they are by 42.8 min and 2.3 A h with the dual-PCM design.

preheating method, Li-ion battery, phase change material, supercooling

Citation: Fang X Y, Nong X L, Liao Z R, et al. A novel preheating method for the Li-ion battery using supercooled phase change materials. Sci China Tech Sci, 2023, 66: 193–203, https://doi.org/10.1007/s11431-022-2209-9

1 Introduction

The Li-ion battery system is now one of the most widely utilized energy storage systems and technologies due to its long life cycle, high power, and high specific energy. The Li-ion battery operates efficiently at optimal operating temperatures ranging from 15 to 35°C, striking a good balance between performance and life [1,2]. Thus, thermal management of the battery management system (BMS) draws excellent attention in academic research.

One of the strategies is BMS based on phase change materials (PCMs) [3]. It can prevent excessive temperature increases that may lead to exothermic reactions and result in thermal runaway [4]. Using PCM's latent heat during melting, the released heat by the battery can be absorbed with a slight temperature rise [5]. For instance, Kim et al. [6] used the commercial PCMs, including RT31, RT15, EG26, and EG5, to explore a PCM-based BMS for the Li-ion battery system. The results showed that the battery with PCM-based BMS achieves a lower temperature rise (30°C) than without PCM (38°C).

Moreover, PCM-based BMS can also deal with performance deterioration in low-temperature conditions. At temperatures below 0°C, the performance of the Li-ion battery

*Corresponding author (email: zhirong.liao@ncepu.edu.cn)

degrades [7]. Chen et al. [8] found that the diffusion rate of lithium ions and the electrochemical reaction rate decreased when the battery was charged and discharged at low temperatures. Then, the internal resistance increases, which leads to lithium-ion deposition and aggravates the aging process. Aris and Shabani [9] revealed that a Li-ion battery's state of charge (SOC) decreased by about 23% when its operating temperature dropped from 25 to −15°C. Therefore, BMS based on PCM with a low phase change temperature has been proposed to prevent the battery from operating at low temperatures [10–12]. Ling et al. [13] compared PCM-free systems with those containing PCM and sought a material that could improve the degrading low-temperature performance of Li-ion batteries. They found that the PCM with high thermal conductivity can effectively uniform the temperature distribution and make the battery performance more consistent. Ghadbeigi et al. [14] showed that the low-temperature performance of commercial PCM modules with graphite/paraffin composites was better than those without PCM after long cold soaks, which saved 9% energy. Ling et al. [15] studied a passive thermal management system with RT28/fumed silica composite PCMs. They found that, compared with the battery without PCMs, the PCM-based battery achieves higher maximum and minimum temperatures and cycle life improves by 76% in the long run.

Furthermore, PCMs are also incorporated with other heating methods in BMS. Zhang et al. [16] proposed a heating strategy attached to PCM and heat films for prismatic batteries. Sandwiched by PCM and heat films on the smaller and larger side surfaces in two heating modes, the battery was heated up from 253 to 283 K. He et al. [17] proposed a PCM-based coupling method for heating the battery with two heat films to keep the temperature in the battery module balanced and guarantee low-temperature preheating. The PCM-based battery module with two heat sheets at 50°C has proven to be the most energy-saving module.

According to the literature review, PCM is utilized in the BMS to maintain the battery temperature at appropriate operating temperatures. However, preheating the battery is also crucial to improve its operating performance. Zhu et al. [18] developed an optimal energy management method for electric vehicles (EVs) powered by Li-ion batteries in a cold environment, revealing that preheating the battery from −10 to 2°C can reduce the vehicle operation cost by 35%. They also concluded that preheating becomes more critical as the ambient temperature drops.

Recently, some research has revealed that PCMs can also preheat the battery by using a supercooling effect. As Sun et al. [10] explained, the PCMs with large supercooling degrees (the temperature difference between the melting and freezing points) can be used to preheat the battery at low temperatures, such as in the harsh environment EVs face during winter in icy regions. When the temperature drops below the phase change temperature, the supercooling effect occurs because the phase-changed lattices cannot form an effective nucleating cluster to stimulate the entire phase change. Thus, the supercooled PCM can store its latent thermal energy at temperatures lower than the theoretical phase transition point. Once applying external activation or further deducing its temperature to the freezing point, the supercooled PCM will solidify and release latent heat. Ling et al. [19] proposed a preheating method based on switching PCMs' supercooling and developed an available strategy of low-temperature heating utilizing PCM's supercooling. The results showed that the warm-up rate of supercooled PCM is faster than the heating rate of supercooled free PCM [20].

It can be seen that PCM-based BMS has been extensively studied. Although effort has been paid, an in-depth analysis of the design, economy and performance improvement for preheating batteries by supercooled PCMs needs further development. Therefore, this study proposes two designs for preheating the Li-ion battery with supercooled PCM. After illustrating the working principles, seven-candidate PCMs with large supercooling degrees are proposed. Moreover, a mathematical model is established to analyze the PCM layer height, thickness, and mass influence on the preheating effect. The economic efficiency of the single-PCM preheating design with different PCMs is discussed. In addition, the optimal aspect ratio of the PCMs' height is studied for the dual-PCM design. Finally, the resulting improvement in battery output performance is evaluated.

2 Physical and mathematical model

2.1 Physical model

Figure 1(a) illustrates the proposed preheating design with a single PCM, called the single-PCM design. Figure 1(b) diagrams the evolution of battery temperature during preheating. Herein, it is assumed that the battery has a uniform temperature distribution in each part and the battery temperature T_b equals the PCM temperature T_{PCM}. Moreover, the effect of anisotropy, as well as heat loss, is neglected. The battery most likely lowers the melting point in autumn and winter. However, the surrounding PCM maintains its liquid state due to the supercooling effect. Once liquid PCM is actuated by external action, it will solidify, releasing latent heat and heating the battery during the preheating process. The actuated action includes adding seed particles of supercooled materials and using external stimuli, like agitation, friction, shock waves, or ultrasonic vibration [11]. Then the battery temperature increases to a higher value with higher output performance for the subsequent process. What warrants special attention is that, as shown in Figure 1(a), the height of PCM may change as needed in the practical design. Besides, such a design can be extended to involve the battery

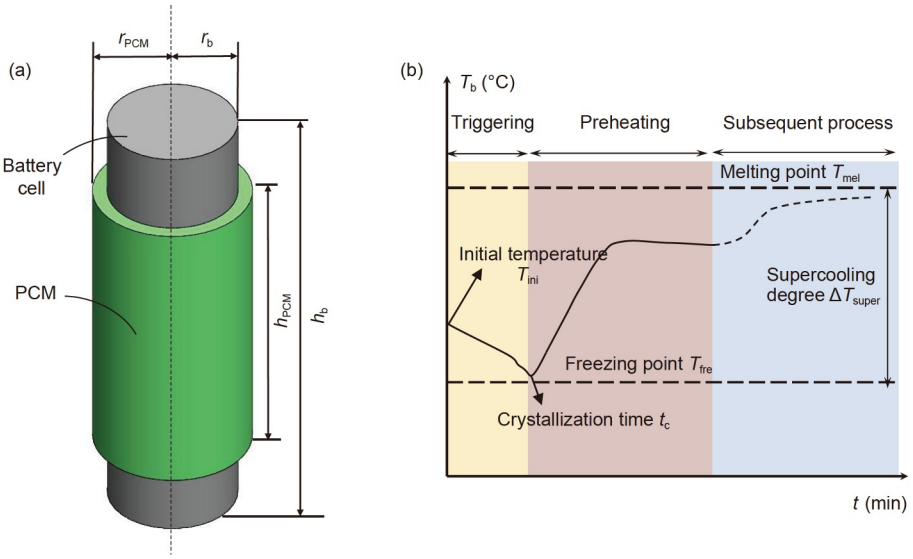

Figure 1 (Color online) (a) The preheating design with a single PCM (the single-PCM design); (b) the diagram of the battery temperature T_b after the PCM triggered.

pack, where the PCM also surrounds the battery pack.

As shown in Figure 1(b), the evolution of battery temperature T_b can be divided into three phases: triggering, preheating and subsequent process. Before triggering, the PCM temperature gradually decreases with the decreasing ambient temperature and becomes lower than its theoretical melting point T_{mel}. Then, the PCM is triggered at the beginning of the preheating process, and the PCM and battery temperature bounces back. According to Yuan et al. [20], a temperature platform would occur during the preheating process. After preheating, the battery can be further warmed up by dissipated heat during operation.

It should be noted that the available temperature range for the single-PCM design is limited. For example, when the area's ambient temperature is below the freezing point, PCM would solidify, and thus the preheating cannot be managed. Thus, the dual-PCM design is proposed, as shown in Figure 2. According to the initial temperature of the battery and the temperature evolution of the intermediate process, the preheating process of the dual-PCM design can be divided into three cases, as shown in Figure 3. In Figure 3, it is assumed that $T_{mel1}<T_{mel2}$ and $T_{fre1}<T_{fre2}$. Furthermore, as illustrated in Figure 3(b) and (c), the stepped temperature trend in the intermediate process can be attributed to PCMs melting [20].

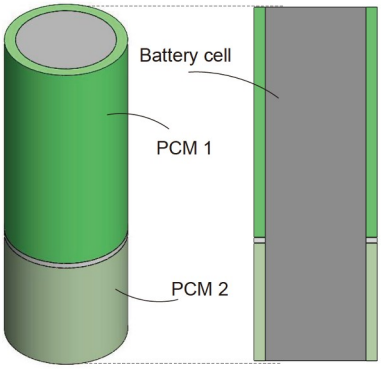

Figure 2 (Color online) The preheating design with dual-PCM (Design 2).

(1) Case 1 (T_{fre1}, $T_{fre2}<T_{ini}$ and $T_{inter}<T_{mel1}$, T_{mel2})

Only PCM2 is activated during the first preheating process in Case 1, as shown in Figure 3(a). During the intermediate process, the battery temperature T_b first increases due to the dissipating heat during discharging. With a short discharging time, T_b does not increase above the melting temperatures of PCM1 or PCM2. After that, T_b decreases because the battery stops working. However, due to supercooling, PCM1 can be triggered in the second preheating. This means that the proposed design can preheat the battery twice.

(2) Case 2 ($T_{fre1}<T_{ini}<T_{fre2}$ and $T_{mel1}<T_{mel2}<T_{inter,max}$)

As shown in Figure 3(b), the initial temperature of battery T_{ini} is lower than T_{fre2}, and PCM2 has solidified. Thus, PCM1 is triggered in the first preheating process. Then, during the intermediate process, T_b increases to higher than T_{mel2}, and both PCM1 and PCM2 melt, indicating that they can be triggered in the second preheating.

(3) Case 3 ($T_{fre1}<T_{ini}<T_{fre2}$ and $T_{mel1}<T_{mel2}<T_{inter,max}$)

For Case 3, shown in Figure 3(c), similar to Case 2, only PCM1 can be activated in the first preheating. Then, T_b increases above T_{mel2} and decreases below T_{fre2} during the intermediate process. Thus, different from Case 2, PCM1 is triggered in the second preheating.

Therefore, the available preheating temperature of the dual-PCM design can be larger than that of the single-PCM design. Besides, the dual-PCM design can preheat the battery twice and shows more flexibility. Such an advantage would be beneficial when an EV needs a second preheating after a

short drive and a stop on a snowy day. It should be noted that the above cases do not include the case where PCM2 is triggered in the first and second preheating. This is because this case is basically the same as the single-PCM design. Despite this, it is noted that Case 3 is attached to the dual-PCM design, because both PCM1 and PCM2 have engaged in the two preheating processes.

2.2 The potential PCMs

Concerning the practical application scenarios and the battery working temperature range, seven potential PCMs for the above preheating design, including $CH_3COONa{\cdot}3H_2O$, $KF{\cdot}4H_2O$, $LiNO_3{\cdot}3H_2O$, $Na_2S_2O_3{\cdot}5H_2O$, $CaCl_2{\cdot}6H_2O$, $Na_4P_2O_7{\cdot}10H_2O$ and Ca $(NO_3)_2{\cdot}4H_2O$, are selected in the present study, as listed in Table 1. From Table 1, it can be concluded that the melting points of those PCMs range from 18.7°C to 70°C. Due to the different supercooling degrees of those PCMs, the freezing points range from −35°C to 0°C.

Thus, if the application scenario's lowest temperature is 0°C, then PCMs with freezing points below 0°C can be used, such as $LiNO_3{\cdot}3H_2O$, $Na_4P_2O_7{\cdot}10H_2O$ and $CaCl_2{\cdot}6H_2O$. If the lowest temperature of the application scenario is −10°C, PCMs such as $Na_2S_2O_3{\cdot}5H_2O$, $KF{\cdot}4H_2O$ and Ca $(NO_3)_2{\cdot}4H_2O$ can be adopted. If the lowest temperature of the application scenario is −20°C, only $CH_3COONa{\cdot}3H_2O$ can be employed.

The following section uses two typical cylindrical batteries, including a 18650-format lithium manganate battery (b1) and a 26650-format lithium iron phosphate battery (b2). Table 2 presents the geometric and physical parameters of those two batteries.

2.3 Mathematical model

To analyze the preheating performance of the above designs, the following assumptions are pursued.

(i) Steady-state.

(ii) Neglecting heat loss and uneven temperature distribution inside the battery.

(iii) The physical properties of PCM are constant at solid and liquid states, respectively.

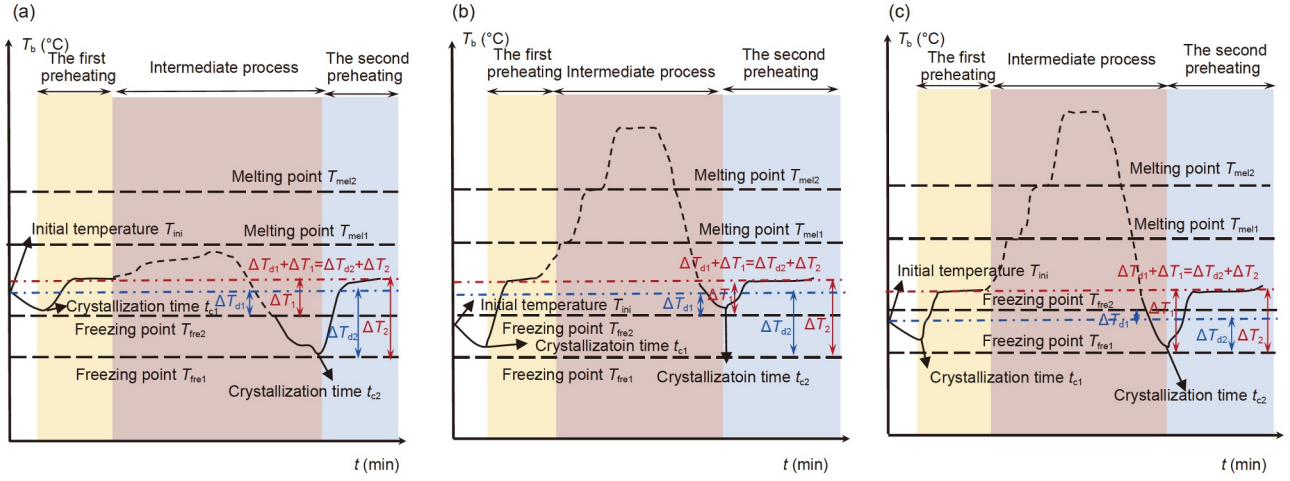

Figure 3 (Color online) The diagram of the evolution of battery temperature T_b during the preheating process under three different conditions. (a) Case 1, PCM2 triggering in the first preheating and PCM1 triggering in the second preheating; (b) Case 2, PCM1 triggering in the first preheating and PCM2 triggering in the second preheating; (c) Case 3, PCM1 triggering in the first and the second preheating.

Table 1 The parameters of phase-change materials by the range of freezing points

Range of the available operating temperature (°C)	0–−10			−11–−20			−21–−35
Symbol	E	C	F	D	B	A	G
Chemical formula	$CaCl_2{\cdot}6H_2O$	$LiNO_3{\cdot}3H_2O$ [21,22]	$Na_4P_2O_7{\cdot}10H_2O$ [21,23]	$Ca(NO_3)_2{\cdot}4H_2O$ [24,25]	$KF{\cdot}4H_2O$	$Na_2S_2O_3{\cdot}5H_2O$ [21]	$CH_3COONa{\cdot}3H_2O$ [21,26]
Density (kg/m^3)	1710 [26]	1575 [27]	1820 [28]	1820	1445 [27]	1750 [29]	1450 [30]
Specific heat capacity (kJ/(kg K))	1.42 [26]	1.30 [31]	3.10 [32]	2.10 [33]	1.84 [29]	1.46 [29,32]	1.70 [29]
Latent heat (kJ/kg)	190 [26]	231 [34]	184 [34]	153 [29]	231.4 [30]	201 [30]	265 [35]
Price per unit of mass (¥/kg)	595 [36]	–	631 [36]	851 [36]	–	481 [36]	403 [36]
Melting point (°C)	29 [34,37]	29.9–30 [27]	70 [34]	47 [34]	18.7 [27]	48 [34]	58 [34]
Sub-cooling point (°C)	30 [34,37]	40 [34]	70 [34]	65 [34]	33 [34]	65 [34]	90 [34]

Table 2 The parameters of battery cells

Battery type	Nominal voltage (V)	Height (mm)	Diameter (mm)	Mass (g)	Density (g/cm^3)	Specific heat capacity (J/(kg K))	Nominal capacity (A h)
b1 (18650-format lithium manganate battery) [38]	3.7	64	18	44.4	2.725	1069.9	2.0
b2 (26650-format lithium iron phosphate battery) [39]	3.2	65	26	78.0	2.059	1375.8	3.0

(iv) Neglecting the heat absorbed by the isolation diaphragms.

Based on the above assumptions, mathematical models are developed to evaluate battery temperature rise for Designs 1 and 2 after preheating.

(1) The single-PCM design

According to the energy balance, the released latent heat $Q_{\text{gen,PCM}}$ is absorbed by the battery $Q_{\text{abs,b}}$ and the PCM $Q_{\text{abs, PCM}}$ in the preheating process:

$$Q_{\text{gen,PCM}} = Q_{\text{abs,PCM}} + Q_{\text{abs,b}}, \tag{1}$$

$$Q_{\text{gen,PCM}} = h_{\text{l,PCM}} r_{\text{PCM}} (r_{\text{PCM}}^2 - r_{\text{b}}^2)\pi h_{\text{PCM}}, \tag{2}$$

$$Q_{\text{abs,PCM}} = C_{\text{PCM}} \rho_{\text{PCM}} (r_{\text{PCM}}^2 - r_{\text{b}}^2)\pi h_{\text{PCM}} \quad T_{\text{b}}, \tag{3}$$

$$Q_{\text{abs,b}} = C_{\text{b}} \rho_{\text{b}} r_{\text{b}}^2 \pi h_{\text{b}} \quad T_{\text{b}}. \tag{4}$$

Substituting eqs. (2)–(4) into eq. (1) yields the temperature rise of the battery ΔT_{b}:

$$T_{\text{b}} = \frac{h_{\text{l,PCM}} \rho_{\text{PCM}} (r_{\text{PCM}}^2 - r_{\text{b}}^2) h_{\text{PCM}}}{C_{\text{b}} \rho_{\text{b}} r_{\text{b}}^2 h_{\text{b}} + C_{\text{PCM}} \rho_{\text{PCM}} (r_{\text{PCM}}^2 - r_{\text{b}}^2) h_{\text{PCM}}}. \tag{5}$$

(2) The dual-PCM design

For the dual-PCM design, when PCM1 is triggered, the released latent heat of PCM1 $Q_{\text{gen,PCM1}}$ is absorbed by the battery and the PCMs:

$$Q_{\text{gen,PCM1}} = Q_{\text{abs,b}} + Q_{\text{abs,PCM1}} + Q_{\text{abs,PCM2}}. \tag{6}$$

Then, similarly to the single-PCM design, the temperature rise of the battery is

$$T_{\text{b}} = \frac{h_{\text{l,PCM1}} r_{\text{PCM1}} (r_{\text{PCM1}}^2 - r_{\text{b}}^2) h_{\text{PCM1}}}{C_{\text{b}} \rho_{\text{b}} r_{\text{b}}^2 h_{\text{b}} + C_{\text{PCM1}} \rho_{\text{PCM1}} (r_{\text{PCM1}}^2 - r_{\text{b}}^2) h_{\text{PCM1}} + C_{\text{PCM2}} \rho_{\text{PCM2}} (r_{\text{PCM2}}^2 - r_{\text{b}}^2) h_{\text{PCM2}}}. \tag{7}$$

When PCM2 is triggered, similar to eq. (6), the released latent heat of PCM2 $Q_{\text{gen, PCM2}}$ is absorbed by the battery and the PCMs:

$$Q_{\text{gen,PCM2}} = Q_{\text{abs,b}} + Q_{\text{abs,PCM1}} + Q_{\text{abs,PCM2}}. \tag{8}$$

Then, the temperature rise of the battery is

$$T_{\text{b}} = \frac{h_{\text{l,PCM2}} r_{\text{PCM2}} (r_{\text{PCM2}}^2 - r_{\text{b}}^2) h_{\text{PCM2}}}{C_{\text{b}} \rho_{\text{b}} r_{\text{b}}^2 h_{\text{b}} + C_{\text{PCM1}} \rho_{\text{PCM1}} (r_{\text{PCM1}}^2 - r_{\text{b}}^2) h_{\text{PCM1}} + C_{\text{PCM2}} \rho_{\text{PCM2}} (r_{\text{PCM2}}^2 - r_{\text{b}}^2) h_{\text{PCM2}}}. \tag{9}$$

It should be noted that according to the assumption (iii), the thermophysical properties of PCMs in the above equations depend on their state of matter.

As shown in eqs. (7) and (9), the battery temperature rise depends on the height of PCM1 and PCM2 (h_{PCM1} and h_{PCM2}) for the dual-PCM design. Herein, a mathematical model based on the non-linear programming GRG method was developed to optimize the ratio of the PCM layer's height for Cases 1–3, as shown in Figure 4. Considering the dual-PCM design can preheat the battery twice, the optimization aims at obtaining the maximum sum of two preheating temperature rises of the battery. Three constraints are set: constraint (1) means the sum of two PCMs' height equals the height of the battery; constraint (2) aims to guarantee that the sum of ΔT_{d} (the difference between T_{ini} and T_{fre}) and ΔT (the difference between T_{fre} and T_{ter}) remains the same for the two preheating processes; and constraint (3) ensures that the battery temperature does not exceed 50°C after preheating. From Figure 4, once the battery height h_{b1}, the thickness of the PCM layer, δ_{PCM}, and the physical properties of PCMs are given, h_{PCM1} and h_{PCM2} can be calculated through the non-linear programming GRG method [40].

(3) Battery performance evaluation after preheating

To evaluate the influence of the preheating on the battery performance, the battery discharging curves are compared under different temperatures. Figure 5 shows the discharging curves of the 18650-format battery (b1) and the 26650-format battery (b2) at 1 C-rate [41,42]. From Figure 5, the discharging time increases with temperature, so the battery can operate longer than that without preheating under the same load. Herein, the prolonged operating time is defined as the time that the battery level elapses from the initial capacity to 80% depth of discharge (DOD) or the cut-off voltage. The saved electricity is defined as the reserved electricity caused by the prolonged operating time. The saved electric quantity (ΔQ_{saved}) for (b1) and (b2) can be calculated by the following express:

$$Q_{\text{saved}} = I \quad t = \left(\frac{C_{\text{a}}}{t}\right) \quad t = C_{\text{a}} \left(\frac{C_{\text{r}}}{3600}\right) \quad t. \tag{10}$$

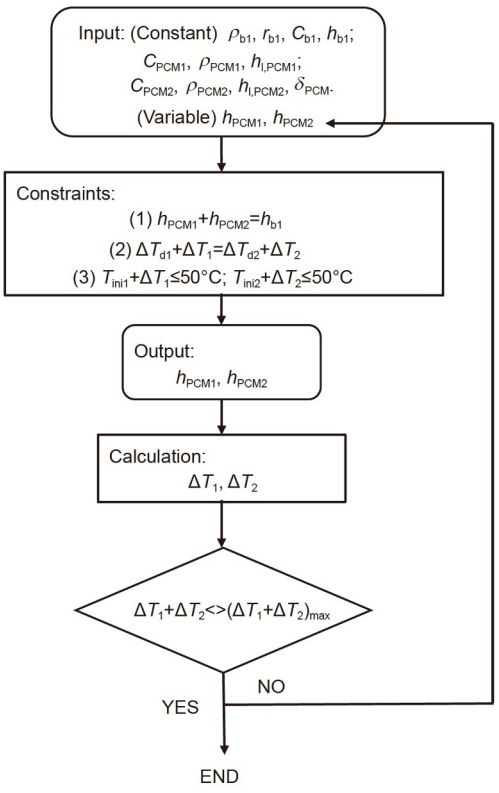

Figure 4 The calculation flow chart of the optimized mathematical model for h_{PCM1} and h_{PCM2}.

3 Results and discussion

3.1 The single-PCM design

In this subsection, the effect of PCM layer dimensions on the preheating effect and the economy is discussed. The 18650-format battery (b1) is used. Besides, for convenience, the initial temperature of the battery is assumed to be greater than the freezing point but lower than the corresponding PCM melting point.

3.1.1 The influence of PCM layer dimensions on the preheating effect

Figure 6 (a) and (b) show the changes in the battery temperature rise ΔT_b with the thickness δ_{PCM} and the height h_{PCM} of the PCM layer for seven different PCMs, respectively. From Figure 6 (a) and (b), it can be seen that the single-PCM design with C ($LiNO_3 \cdot 3H_2O$), G ($CH_3COONa \cdot 3H_2O$), A ($Na_2S_2O_3 \cdot 5H_2O$), E ($CaCl_2 \cdot 6H_2O$) and B ($KF \cdot 4H_2O$), give a larger ΔT_b than that of D ($Ca(NO_3)_2 \cdot 4H_2O$) and F ($Na_4P_2O_7 \cdot 10H_2O$). Among all the seven PCMs, the design with C obtains the highest ΔT_b. When the δ_{PCM} rises from 0.1 to 4.0 mm, ΔT_b of the single-PCM design with C increases from 2.9°C to 80.7°C. When h_{PCM} rises from 20 to 64 mm, the ΔT_b of the design with C increases from 18.3°C to 48.0°C. The small ΔT_b of the single-PCM design with F and D can be attributed to their low latent heat and high specific heat capacities, as listed in Table 1. Besides, it can be seen that the ranking of the seven ΔT_b ($\Delta T_{b,C}>\Delta T_{b,G}>\Delta T_{b,A}>\Delta T_{b,B}>\Delta T_{b,E}>\Delta T_{b,F}>\Delta T_{b,D}$) is not precisely matched with that of their latent heat ($\Delta T_{b,G}>\Delta T_{b,C}>\Delta T_{b,B}>\Delta T_{b,A}>\Delta T_{b,E}>\Delta T_{b,F}>\Delta T_{b,D}$). Thus, it is indicated that when the PCM layer size is fixed, accessing the preheating ability of the single-PCM design only through latent heat may not be a proper strategy.

3.1.2 The PCM's economy

From the above Figure 6(a) and (b), PCM mass rises with the increase in the thickness and the height of the PCM layer. The relationship between the PCM mass and ΔT_b is depicted in Figure 7(a), considering that the mass determines the PCM cost. Furthermore, Figure 7(b) displays the change in total PCM cost $P_{b,pu}$ with the temperature rise ΔT_b for five PCMs. From Figure 7(a), the variation of the PCM mass is accomplished by changing the height of the PCM layer. Besides, the designs with C and B are not presented because their retail prices are unavailable. From Figure 7(a), when the PCM mass equals 8 g, the single-PCM design with G achieves the highest ΔT_b of 34.8°C, while D ranks the lowest

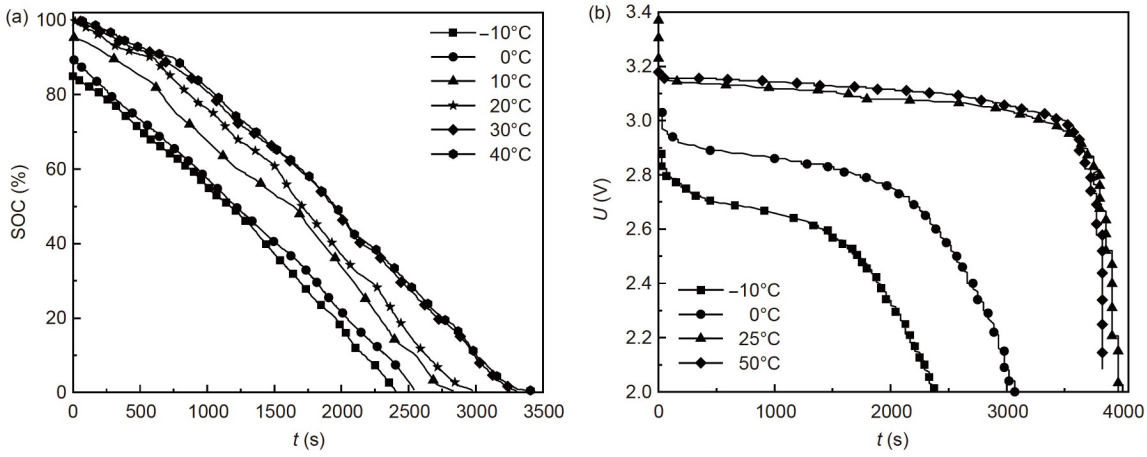

Figure 5 The discharging curves of (a) 18650-format battery and (b) 26650-format battery at different temperatures [41,42].

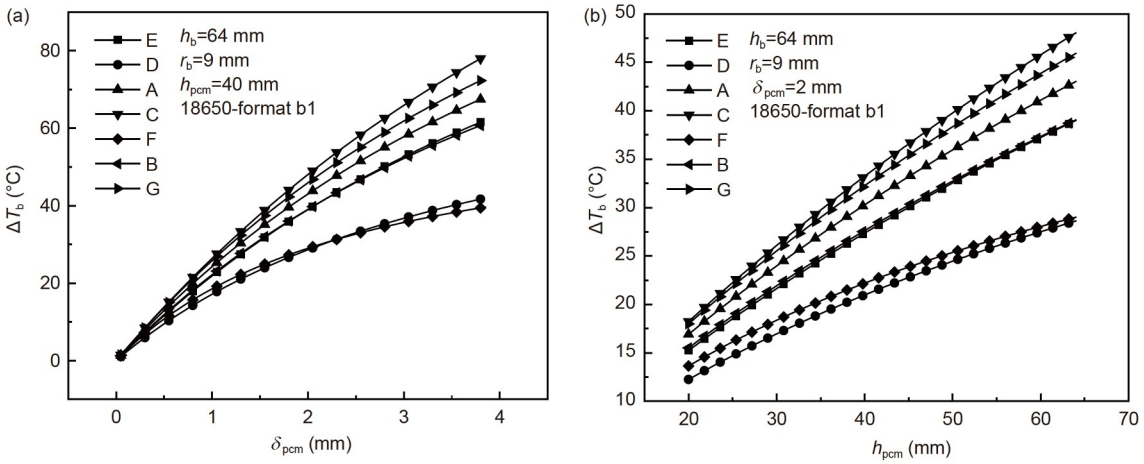

Figure 6 The change of the battery temperature rises ΔT_b with the thickness (a) and height (b) of PCM layer δ_{PCM} for seven PCMs.

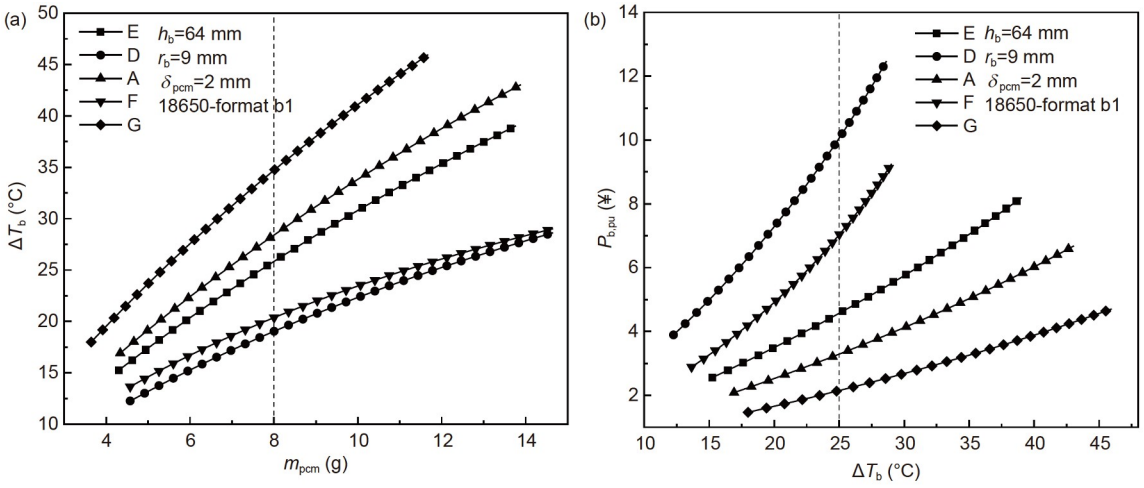

Figure 7 (a) The change of the temperature rises ΔT_b with the increase of mass of PCM layer m_{PCM} for five different PCMs; (b) the change of the total PCM cost $P_{b,pu}$ with the increase of the temperature rises ΔT_b for five different PCMs.

ΔT_b of 19.0 °C. Thus, G has the best preheating ability, while D has the poorest preheating ability. From Figure 7(b), to achieve ΔT_b of 25°C, using G is the more economical (2.2 ¥, CNY), while using D is the most expensive (10.1 ¥, CNY).

Figure 8 compares the levelized temperature rise ΔT_b of each PCM $CP_{b,pu}$ for consuming a cost of 1 ¥, which is calculated from the maximum and minimum slopes of each PCM's ΔT_b vs. $P_{b,pu}$ curve shown in Figure 7(b). From Figure 9, the design with G has the lowest $CP_{b,pu}$ ranging from 12.3 to 9.8°C/¥, followed by A (from 8.1 to 6.4°C/¥) and E (from 6.0 to 4.8°C/¥). While $CP_{b,pu}$ for designs with F (from 4.7 to 3.1°C/¥) and D (from 3.2 to 2.3°C/¥) are the lowest.

From Figures 7 and 8, due to the fact that G, A and E have relatively low density, high latent heat, as well as a low retail price, the single-PCM design with those PCMs achieves not only high ΔT_b but also the economic benefit. Therefore, preheating design using those three PCMs is economical. Additionally, the ranking of $CP_{b,pu}$ is the same as that of ΔT_b shown in Figure 8 ($CP_{b,pu,C}$>$CP_{b,pu,A}$>$CP_{b,pu,E}$>$CP_{b,pu,F}$>$CP_{b,pu,D}$). Since the cost performance $CP_{b,pu}$ is a combination of preheating ability ΔT_b and cost $P_{b,pu}$, it can be concluded that in these five PCMs, the variance in $P_{b,pu}$ is smaller than that in ΔT_b.

3.2 The dual-PCM design

For the dual-PCM design, the selection of PCMs should consider both the freezing point and the preheating ability. Figure 9 shows the maximum temperatures at which those seven PCMs can heat the battery from their corresponding freezing points for the single-PCM design. From Figure 9, it can be seen that different PCMs can heat the battery from their freezing points up to different maximum temperatures. Thus, if two PCMs with considerable differences in freezing points are selected, the dual-PCM design with those two PCMs would produce a wide available temperature range for

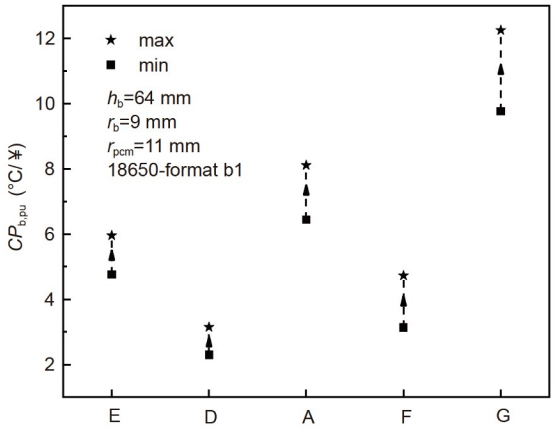

Figure 8 The levelized temperature rise ΔT_b of each PCM $CP_{b,pu}$ for consuming a cost of 1 ¥.

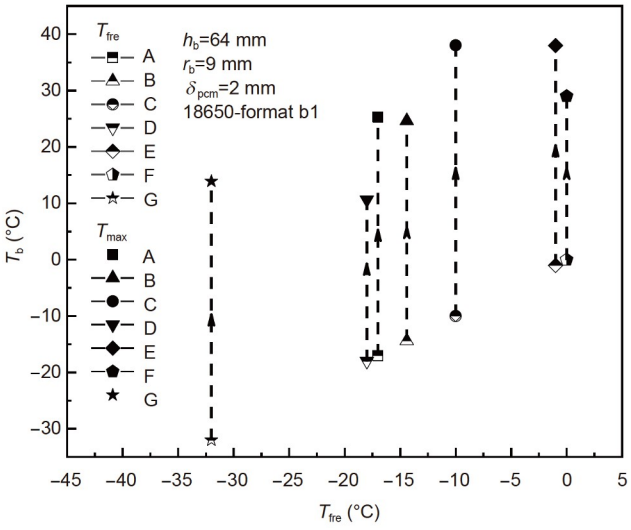

Figure 9 The maximum temperatures T_{max} that those seven PCMs can heat the battery up from their corresponding freezing points T_{fre} for the single-PCM design.

preheating. For instance, from Figure 9, the lowest temperature for preheating with a combination of C and E is −10°C, while the one with the combination of G and E is −30°C.

According to the results in Figure 9, Table 3 lists the potential PCMs for the above three cases of the dual-PCM design. Herein, the 18650-format battery b1 is used; the thickness and height of the PCM layer are 2 and 64 mm, respectively. The last column gives the optimal height percentages for PCM1 and PCM2, obtained by the above-optimized model in Section 2.2. What needs illustration is that the ratios for PCM1 and PCM2 are set to 50% in Case 3, which means half of the PCM layer is triggered for each preheating.

Based on Table 3, Figure 10 shows the maximum temperatures T_{max} that PCMs can heat the battery from their corresponding freezing points T_{fre} in the first and second

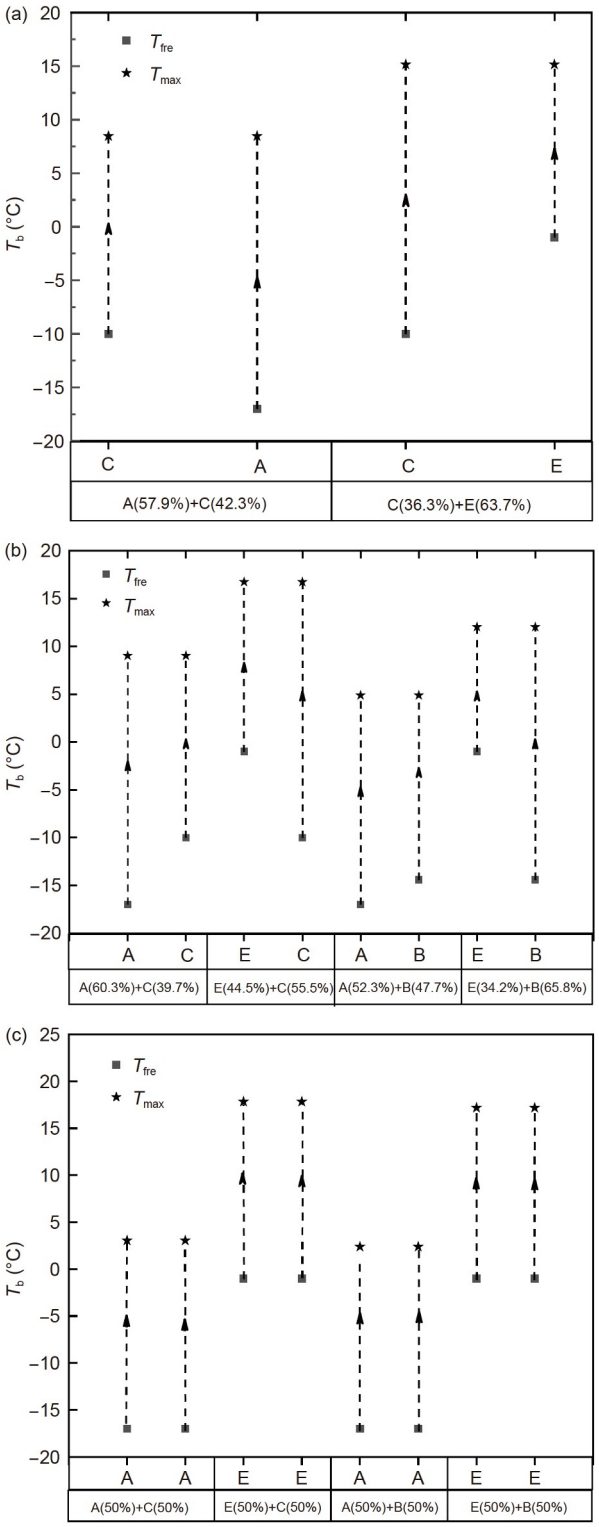

Figure 10 The maximum temperatures T_{max} that the PCMs can heat the battery from their corresponding freezing points T_{fre} in the first and the second preheating processes for Cases 1–3 of the dual-PCM design.

preheating processes for Cases 1–3 of the dual-PCM design. Depending on each PCM's freezing temperature and preheating ability, T_{max} ranges from 5°C to 15°C for Cases 1 and

2 and from 2°C to 23°C for Case 3. Besides, the same set of PCMs can obtain different heating effects for different cases because the thermophysical properties of the PCMs are different, as mentioned before. For example, with C and E, the T_{max} of Cases 1 and 2 are 15°C and 17°C, respectively. It can be seen that the temperature rises of the battery ΔT_b from both the first and the second preheating processes for Cases 1–3 range from 15°C to 32°C, meaning the dual-PCM design can still effectively warm the battery up.

3.3 The improvement of the battery's output performance

The improvement of the battery's output performance with Designs 1 and 2 is discussed in terms of the prolonged operating time and the saved electricity. Both the 18650-format b1 and the 26650-format b2 batteries are discussed. Figure 11 shows the prolonged operating time Δt and the saved electricity ΔQ_{saved} of b1 and b2 for the dual-PCM design with three cases and the single-PCM design with seven different PCMs operating at 1 C_r. According to the battery performance evaluation model presented in Subsection 2.3, Δt and ΔQ_{saved} for the dual-PCM design are the sum of the prolonged operating time and the saved electricity in the first and second preheating processes, respectively.

From Figure 11, Δt ranges from 8.69 to 18.17 min, from 12.19 to 15.54 min, from 18.70 to 57.50 min, and range from 14.02 to 38.80 min for b1 with the single-PCM design, b1 with the dual-PCM design, b2 with the single-PCM design, and b2 with the dual-PCM design, respectively. ΔQ_{saved} ranges from 0.46 to 0.97 A h, from 0.65 to 0.83 A h, from 0.47 to 1.44 A h, and from 0.75 to 2.07 A h for b1 with the single-PCM design, b1 with the dual-PCM design, b2 with the single-PCM design, and b2 with the dual-PCM design, respectively. It can be seen that the fluctuations of Δt and ΔQ_{saved} of b1 with the dual-PCM design are less intense than that with the single-PCM design. For b2, the single-PCM design with four PCMs, including G, C, B and A achieves

Table 3 Potential combinations of PCMs for different cases of the dual-PCM design

Cases of the dual-PCM design	The PCMs		The triggered sequence		Optimal height ratio (%)	
	PCM1	PCM2	The first preheating	The second preheating	h_{PCM1}	h_{PCM2}
Case 1	A	C	C	A	57.9	42.3
	E	C	C	E	63.7	36.3
Case 2	A	C	A	C	60.3	39.7
	E	C	E	C	44.5	55.5
	A	B	A	B	52.3	47.7
	E	B	E	B	34.2	65.8
Case 3	A	C	A	A	50.0	50.0
	E	C	E	E	50.0	50.0
	A	B	A	A	50.0	50.0
	E	B	E	E	50.0	50.0

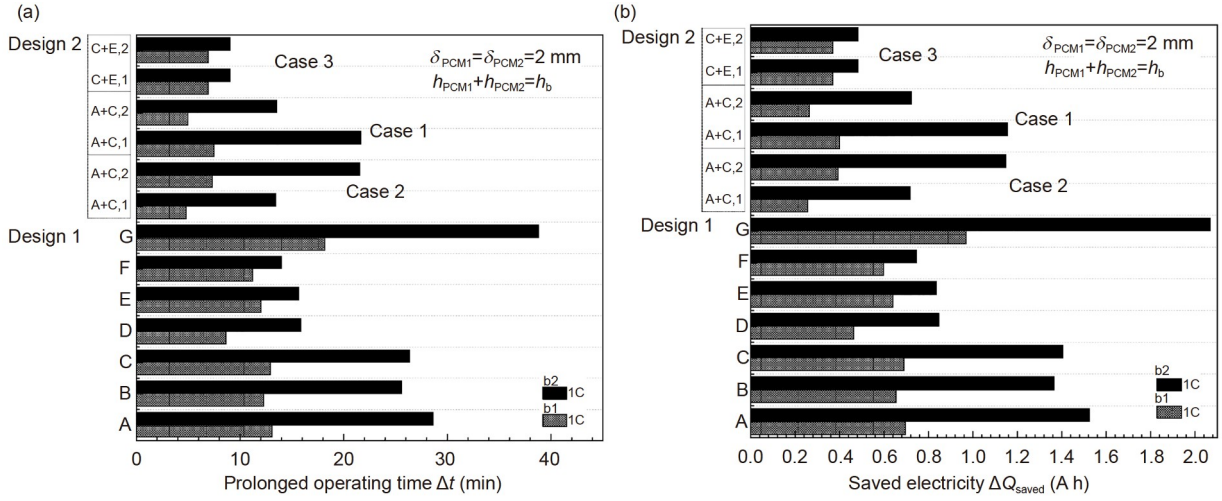

Figure 11 The prolonged operating time Δt (a) and the saved electricity ΔQ_{saved} (b) of b1 and b2 for the dual-PCM design with three cases and the single-PCM design with seven different PCMs, operating at 1 C_r.

higher Δt and ΔQ_{saved} than the dual-PCM design in one preheating process. Whereas the Δt and ΔQ_{saved} summed up in two preheating processes of b2 with the dual-PCM design are higher than that with the single-PCM design in a single preheating process.

4 Conclusions

This study develops a novel preheating method for the Li-ion battery using supercooled PCM. Two specific preheating designs with single- and dual-PCM are proposed, and the effect of PCM layer size on preheating effect and economy is discussed. In addition, the performance improvement of the battery by preheating is evaluated. The main findings of the study are listed as follows.

(1) Using available PCMs, the proposed preheating designs have an operating temperature range from −30°C to 20°C. The preheating designs can warm up the battery by as high as dozens of degrees Celsius and improve battery output performance by more than 0.2 A h.

(2) Accessing the preheating ability of PCMs only through PCM's latent heat may not be the right strategy. For using $LiNO_3 \cdot 3H_2O$, $CH_3COONa \cdot 3H_2O$, $Na_2S_2O_3 \cdot 5H_2O$, $CaCl_2 \cdot 6H_2O$ and $KF \cdot 4H_2O$ as PCMs can obtain much higher preheating ability than using $Ca(NO_3)_2 \cdot 4H_2O$ and $Na_4P_2O_7 \cdot 10H_2O$. Besides, the design with $CH_3COONa \cdot 3H_2O$ is the most economical, followed by $Na_2S_2O_3 \cdot 5H_2O$ and $CaCl_2 \cdot 6H_2O$.

(3) The dual-PCM design cannot provide a better preheating ability, but it can preheat the battery twice at temperatures over ten degrees Celsius each time. Besides, the total prolonged operating time and the total saved electrical quantity of the two preheating processes for the dual-PCM design are larger.

Further work can be done to study the complete operating processes of the preheating design, including the PCM's solidified and melting processes, testing the actual performance of potential PCMs, and investigating the external action triggering the PCM.

This work was supported by the National Natural Science Foundation of China (Grant Nos. 51821004, 51876061) and the Interdisciplinary Innovation Program of North China Electric Power University.

1 Pesaran A, Santhanagopalan S, Kim G H. Addressing the impact of temperature extremes on large format Li-ion batteries for vehicle applications (Presentation). United States, 2013-05-01, 2013
2 Pesaran A A. Battery thermal models for hybrid vehicle simulations. J Power Sources, 2002, 110: 377–382
3 Bibin C, Vijayaram M, Suriya V, et al. A review on thermal issues in Li-ion battery and recent advancements in battery thermal management system. Mater Today-Proc, 2020, 33: 116–128
4 Wang Q, Ping P, Zhao X, et al. Thermal runaway caused fire and explosion of lithium ion battery. J Power Sources, 2012, 208: 210–224
5 Lin X, Zhang X. Research progress of phase change storage material on power battery thermal management. Energy Tech, 2021, 9: 2000940
6 Kim S W, Talluri T, Angani A, et al. Improve performance of the lithium polymer battery module Part 1: Heat transfer enhancement on Li-pouch battery with PCM in hot soaking. In: Proceedings of the 2020 IEEE 2nd International Conference on Architecture, Construction, Environment and Hydraulics (ICACEH). Hsinchu, Taiwan, China, 2020. 87–89
7 Ma S, Jiang M, Tao P, et al. Temperature effect and thermal impact in lithium-ion batteries: A review. Prog Nat Sci-Mater Int, 2018, 28: 653–666
8 Bing B, Zheng L, Li X, et al. Discharge performance and charge-discharge heat generation characteristics of aging batteries (in Chinese). Energy Storage Sci Technol, 2022, 11: 679–689
9 Aris A M, Shabani B. An experimental study of a lithium ion cell operation at low temperature conditions. Energy Procedia, 2017, 110: 128–135
10 Sun M, Liu T, Li M, et al. A deep supercooling eutectic phase change material for low-temperature battery thermal management. J Energy Storage, 2022, 50: 104240
11 Safari A, Saidur R, Sulaiman F A, et al. A review on supercooling of phase change materials in thermal energy storage systems. Renew Sustain Energy Rev, 2017, 70: 905–919
12 Bayern Z. Storage technology issues and opportunities. In: Proceedings of the Committee on Energy Research and Technology (International Energy Agency), International Low-Carbon Energy Technology Platform, Strategic and Cross-Cutting Workshop "Energy Storage-Issues and Opportunities". Paris, 2011
13 Ling Z, Wen X, Zhang Z, et al. Thermal management performance of phase change materials with different thermal conductivities for Li-ion battery packs operated at low temperatures. Energy, 2018, 144: 977–983
14 Ghadbeigi L, Day B, Lundgren K, et al. Cold temperature performance of phase change material based battery thermal management systems. Energy Rep, 2018, 4: 303–307
15 Ling Z, Wen X, Zhang Z, et al. Warming-up effects of phase change materials on lithium-ion batteries operated at low temperatures. Energy Technol, 2016, 4: 1071–1076
16 Zhang J, Liu H, Zheng M, et al. Numerical study on a preheating method for lithium-ion batteries under cold weather conditions using phase change materials coupled with heat films. J Energy Storage, 2022, 47: 103651
17 He F, Li X, Zhang G, et al. Experimental investigation of thermal management system for lithium ion batteries module with coupling effect by heat sheets and phase change materials. Int J Energy Res, 2018, 42: 3279–3288
18 Zhu T, Min H, Yu Y, et al. An optimized energy management strategy for preheating vehicle-mounted Li-ion batteries at subzero temperatures. Energies, 2017, 10: 243
19 Ling Z, Luo M, Song J, et al. A fast-heat battery system using the heat released from detonated supercooled phase change materials. Energy, 2021, 219: 119496
20 Yuan K, Zhou Y, Sun W, et al. A polymer-coated calcium chloride hexahydrate/expanded graphite composite phase change material with enhanced thermal reliability and good applicability. Compos Sci Tech, 2018, 156: 78–86
21 Lane G A. Solar Heat Storage: Latent Heat Materials, Vol II—Technology. Chicago: CRC Press, 1986
22 Shamberger P J, Reid T. Thermophysical properties of lithium nitrate trihydrate from (253 to 353) K. J Chem Eng Data, 2012, 57: 1404–1411
23 Zalba B, Marın J M, Cabeza L F, et al. Review on thermal energy storage with phase change: Materials, heat transfer analysis and applications. Appl Thermal Eng, 2003, 23: 251–283
24 Sharma A, Tyagi V V, Chen C R, et al. Review on thermal energy storage with phase change materials and applications. Renew Sustain Energy Rev, 2009, 13: 318–345

25 Pacák P. Crystal growth from a calcium nitrate tetrahydrate melt. *Kristall und Technik*, 1980, 15: 523–529
26 Günther E. Sononucleation of inorganic phase change materials. Dissertation of Doctoral Degree. München: Technische Universität München, 2011
27 Hirschey J R, Kumar N, Turnaoglu T, et al. Review of low-cost organic and inorganic phase change materials with phase change temperature between 0°C and 65°C. In: International High Performance Buildings Conference at 2020 Herrick Conferences. West Lafayette, 2021
28 https://www.nwmissouri.edu/naturalsciences/sds/p/Pyrophosphate%20tetrasodium%20decahydrate.pdf. Available online (accessed on 2022.07.27)
29 Purohit B K, Sistla V S. Inorganic salt hydrate for thermal energy storage application: A review. Energy Storage, 2021, 3: e212
30 Hirschey J, Gluesenkamp K R, Mallow A, et al. Review of inorganic salt hydrates with phase change temperature in range of 5 to 60° C and material cost comparison with common waxes. In: International High Performance Buildings Conference. West Lafayette, 2018
31 Luo C, Su Q, Mi W. Thermophysical properties and application of $LiNO_3$-H_2O working fluid. Int J Refrig, 2013, 36: 1689–1700
32 Yim C, Choi K, Kim J, et al. A study of heat transfer characteristics of PCM in a latent heat storage tank (cubic type). Solar Energy, 1995, 15: 15–27
33 Sádovská G, Honcová P, Pilař R, et al. Calorimetric study of calcium nitrate tetrahydrate and magnesium nitrate hexahydrate. J Therm Anal Calorim, 2016, 124: 539–546
34 Beaupere N, Soupremanien U, Zalewski L. Nucleation triggering methods in supercooled phase change materials (PCM), a review. Thermochim Acta, 2018, 670: 184–201
35 Fang G, Zhang W, Yu M, et al. Research progress of phase change energy storage materials $CH_3COONa·3H_2O$ (in Chinese). New Chem Mater, 2021, 49: 16–20
36 https://www.chemicalbook.com/ProductIndex.aspx. Available online (accessed on 2022.07.27)
37 Cao F, Zheng Y, Chen C H, et al. Thermal energy storage with tunable melting point phase change materials. In: Proceedings of the International Heat Transfer Conference. Digital Library, 2018
38 Fang Z, Maode L. Study on temperature rise effect of cylindrical lithium-ion battery (in Chinese). Power Technol, 2011, 35: 1061–1062, 1068
39 Jiang G. Preparation of high thermal conductivity composite phase change materials and application research on thermal management of power batteries (in Chinese). Dissertation of Doctrol Degree. Nanchang: Nanchang University, 2017
40 Geem Z W, Noh J S. Parameter estimation for a proton exchange membrane fuel cell model using GRG technique. Fuel Cells, 2016, 16: 640–645
41 Niu X, Tian J, Zhao F, et al. Estimation of SOC of Li-ion battery under different ambient temperature (in Chinese). First Battery Bimonthly, 2021, 51: 342–345
42 Zhan S, Tang N, Wang J. Research on SOC estimation method of $LiFePO_4$ battery (in Chinese). Chin J Power Sources, 2015, 39: 1620–1622